Composites Part A **29A** (1998) 1063–1070
1359-835X/98/$ - see front matter

PII: S1359-835X(98)00046-3

Measurement and analysis of stress transfer and toughness at a fiber–matrix interface

A. Pegoretti* and A.T. DiBenedetto
Institute of Materials Science and Department of Chemical Engineering, University of Connecticut, Storrs, CT 06269, USA

The finite element method is used to investigate the axial fiber stress profiles and energy changes accompanying interfacial debonding and/or matrix cracking following a single fiber fragmentation event. Since the stress transfer along the fiber length changes over a long distance from the broken fiber end, a study was made of the effect of model size and material properties on calculated values of the stress profiles and energy changes. The radial dimension must extend to at least 10 fiber diameters and the half-fragment length must also be greater than approximately 20 fiber diameters, before a size independent calculated value of the strain energy release rate, *G*, can be attained. Some of the static-elastic analysis limitations, i.e. the elastoplastic behavior of the matrix, the transient dynamic events following filament fracture, and the frictional effects are also discussed. © 1998 Published by Elsevier Science Ltd. All rights reserved

(Keywords: B. fracture toughness; interface/interphase; finite element method)

INTRODUCTION

The durability of fiber reinforced composite materials is affected by environmental factors such as temperature, moisture and the state of stress to which the material is exposed. The interfacial properties are of paramount importance since damage most often initiates and propagates from changes at the fiber–matrix interfaces. Under usual service conditions, a composite will experience cyclic loads and a changing environment. Inevitably, individual filaments will fracture at low loads relative to the ultimate strength of the material. These fractures are the precursors of critical levels of damage. When a continuous filament fractures, the stored elastic energy lost by the constituents in the region around the broken fiber ends is sufficient to propagate cracks into the matrix and/or along the interface. The precise mode of failure is often a function of the environmental conditions and time, thus complicating the prediction of long-term behavior. A number of research groups have characterized the resistance to propagation of these defects by combining experimental observations of filament fracture in embedded single fiber microcomposites with either analytical solution or finite element analysis of the stress transfer and energy changes accompanying the fracture of an embedded filament[1–9].

In recent publications, we have used the embedded single fiber test to measure the energy changes accompanying the initiation, propagation and arrest of interfacial debonding and matrix cracking immediately following the first fiber fracture[4,9,10]. The test specimen was loaded to the initiation of first fiber fracture and the arrested states of the interface and matrix cracks formed at the end of the broken fiber were observed. By calculating the equilibrium energy states at the beginning and end of the process, the strain energy release rates at the point of arrest, *G*, of the fracture processes were evaluated. Assumptions were made which beg the question of the validity of considering the calculated values of fracture energy as true material properties, independent of the state of stress of the test specimens. Nairn has pointed out the inadequacies of one-dimensional models and shear yielding criteria[2]. Interpretation of his analytical work also leads to the conclusion that ''*damage zones*'' are likely to extend a long distance from the broken fiber end, thus requiring the use of very large models to estimate adequately the total energy changes accompanying a fracture event at a broken fiber end. In addition, friction losses when the broken fiber retracts into the matrix[10], acoustic energy losses generated by fracture events[11], viscoelastic behaviour of the matrix[6], and the kinetic energy of the moving cracks[12] all contribute to a complete energy balance. but are often ignored.

The objective of this work is to present a parametric study of a finite element model for the calculation of axial fiber stress and energy change accompailying an interfacial debonding and/or matrix cracking following a single fiber fragmentation event. The efficiency of the stress transfer will be characterized in the light of the concept of imperfect interface damage parameters [1,2] and a dynamic fracture toughness, $G_{DYNAMIC}$, for the process will be defined using

* Corresponding author. On leave from University of Trento, Department of Materials Engineering, via Mesiano 77, 38050 Trento, Italy.

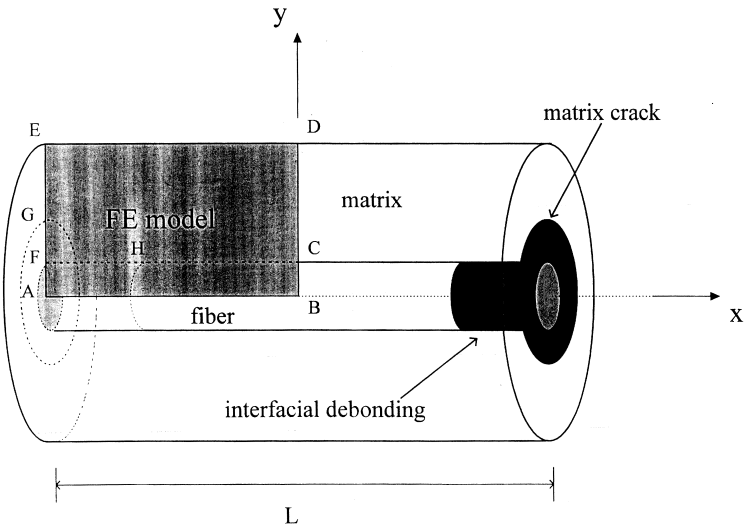

Figure 1 Cylinder of matrix material surrounding a single filament fragment of length L. The region ABDE represents the FE mesh (one quarter of the model). The model dimensions are AB = X and BD = Y

the observed dimensions of the defects upon arrest at constant strain. A case study is presented using S-glass and E-glass single filaments treated with different sizing and/or coupling agents embedded in epoxy matrices of different moduli. Samples were mounted under an optical microscope and loaded until a single fiber fracture occurred. The strain-at-break was monitored and, at constant strain, the fracture emanating from the broken fiber end was observed and its dimensions measured. An axisymmetrical finite element model was used to simulate the experiments and calculate the axial fiber stresses and the strain energy changes accompanying the observed fracture mode. Details of the experimental procedures and results using a linear elastic model were presented in a previous publication[3].

THE FINITE ELEMENT MODEL

The stress profiles and the change in elastic strain energy associated with debonding and matrix cracking accompanying a filament fracture are evaluated using an axisymmetrical finite element (FE) model similar to that previously reported [4,9–11,13,14]. The fragmentation process is modeled as a cylinder of matrix material surrounding a single filament fragment of length, L (*Figure 1*). Simulation is carried out on one quadrant of the cylinder with (AB) and (BDC) as the axes of symmetry. The commercial FE package MARC (MARC Analysis Research Corporation) is used to generate a mesh consisting of four-nodes quadrilateral axisymmetric elements with an aspect ratio varying from 1 to 4. The following boundary conditions are chosen:

(1) side (AB)—displacement equal to zero in the y direction;
(2) side (DE)—free surface;
(3) side (AFE)—displacement equal to zero in the x direction (filament fracture along this plane);
(4) side (BCD)—prescribed uniform displacement in the x direction.

Fiber breakage is simulated by releasing the boundary condition on the side (AF) to produce a free surface. Different damage patterns are simulated by deleting appropriate mesh elements or by using suitable boundary conditions. In particular, the interfacial debonding was simulated by releasing duplicate nodes along the line FH of the model, while the matrix crack damage was simulated by removing the boundary condition on the nodes along the line FG. The boundary condition (4) implies that the solutions are for an infinitely long fiber with a periodic array of equally spaced filament fractures. Experiments were conducted only to the point of first filament fracture. Since the stress transfer along the fiber length changes over a long distance from the broken fiber end, a study was made of the effect of model size on calculated values of the stress profiles and energy changes.

Calculations were made over a range of half length of the filament of:

$$50\ \mu\text{m} < AB = X < 1600\ \mu\text{m}$$

and radius of the cylindrical matrix of:

$$30\ \mu\text{m} < AE = Y < 200\ \mu\text{m}$$

The ratio of fiber and outer radii dimensions defines the fiber volume fraction of the model, which also affects calculated values of the strain energy release rates. The range of fiber and matrix properties used are as follows:

$$\text{S} - \text{glass},\ E_\text{f} = 86.9\ \text{GPa},\ \nu_\text{f} = 0.22,\ d_\text{f} = 10\ \mu\text{m}$$

$$\text{E} - \text{glass},\ E_\text{f} = 72.0\ \text{GPa},\ \nu_\text{f} = 0.22,\ d_\text{f} = 14\ \mu\text{m}$$

$$1 < \text{fiber/matrix modulus ratio} < 869$$

A linear-elastic analysis is carried out at 1% strain, ($\varepsilon = 0.01$) since all stresses will be proportional to ε and all energies proportional to ε^2. The total stored elastic energy, U_E, at 1% strain was plotted as a function of crack length, and a strain energy release rate, G, was determined from the relation: $G = -(\text{d}U_\text{E})/(\text{d}A)$. Elastoplastic analysis is carried

out, for illustration, at specifically observed conditions of strain and defect dimensions. An appropriate energy balance for a growing crack of surface area, A, contains the following terms:

$$\frac{dW_{EXT}}{dA} - \frac{dU_E}{dA} - \frac{dE_{KIN}}{dA} - \frac{dW_{IRR}}{dA} = 0 \qquad (1)$$

where W_{EXT} is the external work done by the system, U_E is the strain energy released, E_{KIN} is the kinetic energy of the moving crack and W_{IRR} is the total energy absorbed irreversibly by viscous dissipation, friction and transient acoustic emission. The parametric study is limited to:

$$\frac{dW_{EXT}}{dA} - \frac{dU_E}{dA} = G = \text{strain energy release rate} \qquad (2)$$

In this case, it is assumed that, $G = G_c = R = (dW_{IRR})/(dA)$ where R is the resistance to the propagation of an existing, slowly propagating crack (i.e. $(dE_{KIN})/(dA) = 0$).

Experimental measurements of the dimensions of arrested cracks under conditions of constant strain will be used to illustrate the simulation technique.

It is important to point out, however, that the experiment is conducted by slowly loading the embedded single filament microcomposite until the first fiber fracture occurs. As it has been described in a previous publication[11], the debonding and matrix cracking following the fracture occur, and arrest, within nanoseconds. This dynamic process contains both kinetic and acoustic energy changes that are not considered in the above analysis. Therefore, for the dynamic initiation, growth and arrest of the observed defects:

$$G - \frac{dE_{KIN}}{dA} - \frac{d\hat{W}_{IRR}}{dA} = 0 \qquad (3)$$

and the measured value of G using the above analysis, $G_{DYNAMIC}$, is not equal to G_c, since $\hat{W}_{IRR} \neq W_{IRR}$ and the kinetic energy of the growing crack will result in the crack arresting at a length somewhat greater than expected from static equilibrium conditions (i.e. $G_{DYNAMIC} \neq G_C$)[12]. This situation is akin to traditional impact testing. While the measurements are relevant, the resulting calculations cannot result in a true material property that is independent of the stress state of the material.

The effects of neglecting plastic deformation of the matrix and friction occuring when the broken fiber end retracts into the matrix will also be presented for specific cases.

RESULTS AND DISCUSSION

A parametric study of the strain energy release rate for debonding and matrix crack propagation

Figure 2(a) and (b) illustrates typical plots of G versus debond and matrix crack length at 1% constant strain calculated using a linear elastic FE model with dimensions $X = 200$ μm, $Y = 100$ μm, an S-glass fiber of diameter $d_f = 10$ μm and an elastic matrix with a modulus of 2.70 GPa. *Figure 3* illustrates the effect of the model dimensions, X and Y, on the calculated value of G for a specific crack length of 16.5 μm for an S-glass fiber embedded in an elastic matrix with a modulus of 1.35 GPa. This plot is typical of the calculations for all of the systems examined. It is clearly seen that the model dimensions have a significant effect on the calculated values. The radial dimension must extend to at least $Y = 100$ μm, or 10 fiber diameters, before a size independent calculated value of G can be attained. With $Y > 100$ μm, the half-fragment length must also be greater than approximately $X = 200$ μm, or 20 fiber diameters, to obtain a truly size independent calculated value of G. This illustrates that changes in the stress transfer extend at least 20 fiber diameters from the fragment end, consistent with analytical calculations using Bessel–Fourier analysis[2] and shear lag analysis[3,15]. *Figure 4* shows that in this range G is proportional to the fiber volume fraction, $V_f = (r_f/Y)^2$, and may be extrapolated easily to zero volume fraction. (We suggest that the extrapolated value may serve as a useful reference state for comparison of G values for different systems.) All subsequent calculations of G using a linear elastic FE model will be made using models with $X/d_f = 20$ and $Y/d_f = 10$. *Figure 5* shows the effect of E_f/E_m on the elastic strain energy release rate, at 1% strain,, at the point of arrest of a 5.5 μm debond initiated at the end of an S-glass filament fracture. As seen in *Figures 3* and *4*, G becomes approximately independent of sample geometry when $X > 40$ and $Y > 10$ or, in other words, the derivative

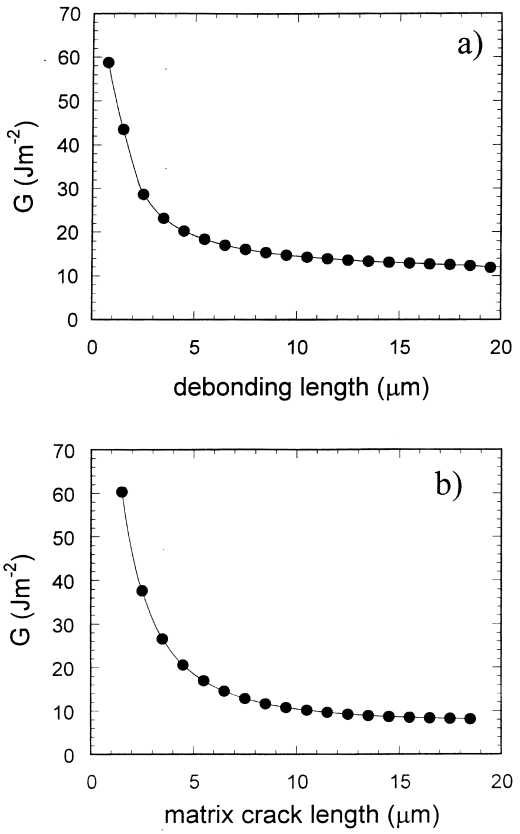

Figure 2 Plots of G versus (a) debond and (b) matrix crack length at 1% strain for a linear-elastic FE model with dimensions AB = $X = 200$ μm and BD = $Y = 100$ μm and a fiber diameter of 10 μm. Fiber and matrix modulus are 86.9 and 2.70 GPa, respectively

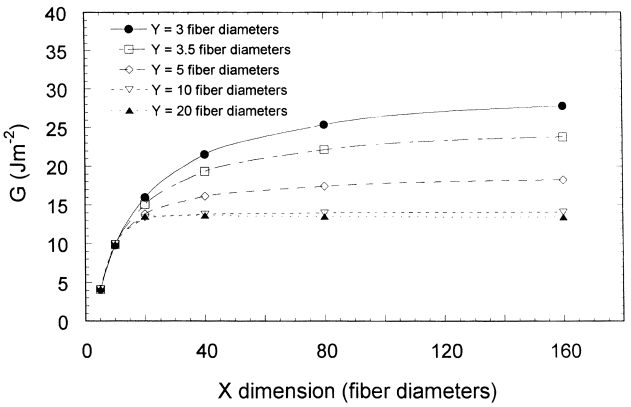

Figure 3 Effect of model dimensions (*X* and *Y*) on the calculated value of G at 1% strain for a specific debonding length of 165 μm. Fiber and matrix modulus are 86.9 and 1.35 GPa, respectively

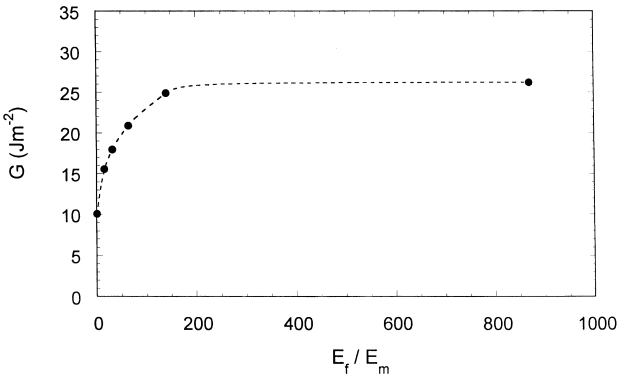

Figure 5 Effect of the ratio of fiber to matrix modulus on the strain energy release rate for the formation of a 5.5 μm debond at a S-glass broken fiber end. The analysis is linear elastic and the model size is $X = 40$ fiber diameters, $Y = 10$ fiber diameters, $d_f = 10$ μm

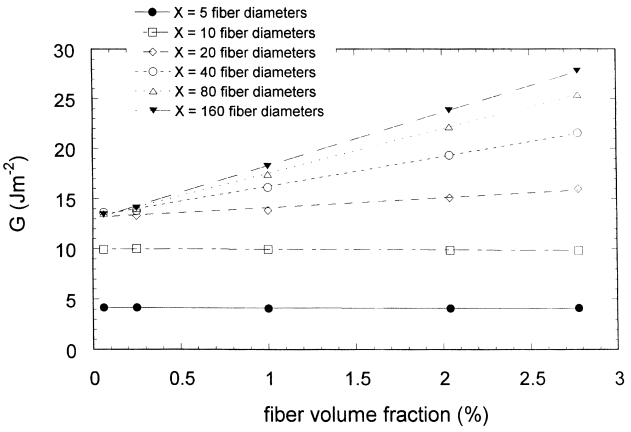

Figure 4 Effect of the fiber volume fraction on the calculated value of *G* at 1% strain for a specific debonding length of 16.5 μm. Fiber and matrix modulus are 86.9 and 1.35 GPa, respectively

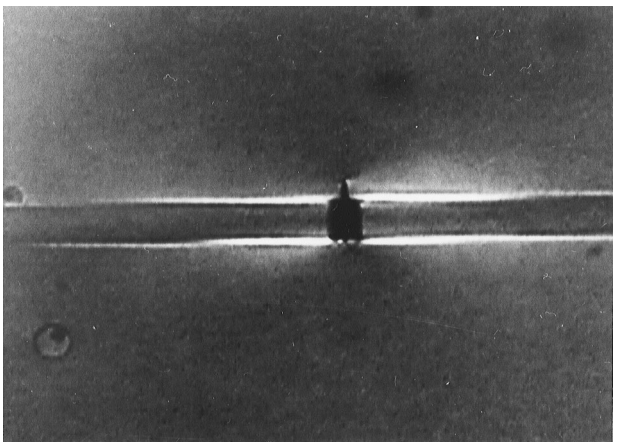

Figure 6 Example of the fracture patterns at a broken fiber end. Commercial epoxy-compatible sized S-glass fiber embedded in an epoxy matrix

$(dU_E)/(dA)$ is approximately constant for a given fiber–matrix combination. However, the magnitude of the stored strain energy, U_E, in the test specimen and the contributions of the two phases to the strain energy release rate, *G*, as calculated by the finite element analysis, are functions of the modulii of the two components. Filament fracture and debonding produces an isolated fragment whose stress bearing capacity depends on stress transfer from the matrix to the fiber. The lower the matrix modulus. the lower will be the stored elastic energy in the fiber fragment relative to that in a segment of the continuous filament. Thus, as E_f/E_m increases, the greater will be the release of strain energy from the S-glass fiber, the more the resulting fragment will retract in the matrix phase and the greater will be the local deformation of the matrix phase at the fiber end. For the composite described in *Figure 5*, below E_f/E_m equal to approximately 200, the total elastic strain energy release rate during debonding, *G*, increases as the matrix modulus and the stress transfer efficiency to the fiber decreases. When E_f/E_m is greater than 200, *G* becomes less sensitive to a reduction of E_m. As the matrix modulus approaches very low values, the finite element analysis becomes irrelevant, since the total stored elastic energy in the specimen becomes negligible at the instant following filament fracture.

A parametric study of the fiber efficiency after debonding and/or matrix cracking

The average axial fiber stress in a fiber fragment has been used as a measure of fiber efficiency in composite materials[16,17]. The efficiency of stress transfer to a fiber fragment was defined as the average axial fiber stress in the fragment, divided by the axial fiber stress carried by an infinitely long continuous filament, i.e. $< \sigma_f >_{fragment} / < \sigma_f >_{continuous\ filament}$. where $< \sigma_f >$ is the average axial fiber stress. The imperfect interface parameter, D_s[2], and the cumulative stress transfer function, CSTF[6], are obtained from analytical models that more precisely define this property. In many cases, interfacial damage is more complex than that assumed in available analytical models, for example, when combinations of interface debonding and matrix cracking occur, as shown in *Figure 6*. Finite element analysis is useful in such cases for calculating the average axial fiber stress. *Figure 7* compares

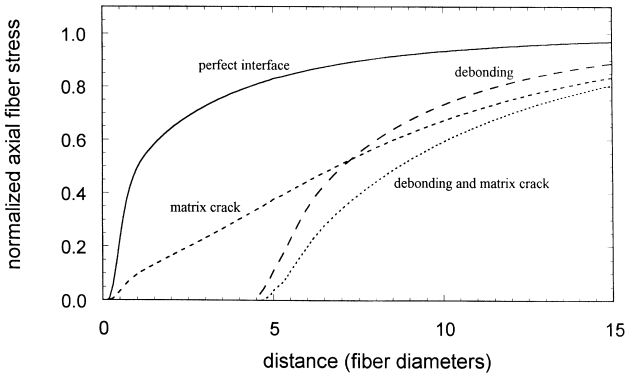

Figure 7 Effect of an imperfect interface (debonding and/or matrix crack) on the axial fiber tensile stress in a single S-glass fiber embedded in an elastic matrix with a modulus of 2.70 GPa, at 1% of strain. All stresses have been normalized to the far-field axial fiber stress. The model size is $X = 50$ fiber diameters, $Y = 10$ fiber diameters, $d_f = 10\ \mu$m, debond and matrix crack length are equal to 5 fiber diameters

Table 1 Reduced axial average fiber stress ($< \sigma_f >_{RED}$) and average axial fiber stress ($< \sigma_f >_{damaged}$) at 1% strain for various damage patterns for an S-glass fiber fragment embedded in elastic matrices with elastic modulus $E_m = 2.7$ GPa. The FE model dimensions are $X = 50$ fiber diameters, $Y = 10$ fiber diameters, $d_f = 10\ \mu$m.

	Defect size (μm)	$< \sigma_f >_{RED}$	$< \sigma_f >_{damaged}$ (MPa)
Perfect interface	0	∞	815.8
Interfacial debond	5	48.1	799.2
	10	26.2	785.2
	20	14.7	763.7
	50	6.4	706.1
	500	0	0
Matrix crack	5	35.9	793.7
	10	22.9	781.7
	20	14.2	762.1
	50	6.0	699.9
Debond and matrix crack	5	31.4	790.6
	10	18.9	774.9
	20	10.9	747.4
	50	4.2	660.2

the normalized axial stress profile at 1% strain near the end of a broken filament (S-glass fragment of length $L = 100$ fiber diameters, $d_f = 10\ \mu$m, in a matrix of modulus $E_m = 2.70$ GPa), of an undamaged (perfect) interface with those having a debond, matrix crack or a combination of both defects. The average axial fiber stress is a function of the lengths of both the interfacial debond and the matrix crack. When both defects are present, the profiles are different than those with only a single defect, as expected. The rate of change of the stress at the broken fiber end is a measure of the ''perfection'' of the interface in that region. One can express the fiber fragment efficiency in any of the above-mentioned formats. In *Table 1* we report the average axial fiber stress, $< \sigma_f >_{damaged}$, computed as:

$$< \sigma_f >_{damaged} = \frac{1}{L}\int (\sigma_f)_{damaged} dL \qquad (4)$$

where (σ_f) is the axial fiber stress at point x along the fiber length, and a reduced axial average fiber stress, as $< \sigma_f >_{RED}$ as:

$$< \sigma_f >_{RED} = \frac{< \sigma_f >_{damaged}}{< \sigma_f >_{undamaged} - < \sigma_f >_{damaged}} \qquad (5)$$

The average axial fiber stress, $< \sigma_f >$, is the same as that proposed by Tripathy and Jones[6]. The reduced average axial fiber stress, $< \sigma_f >_{RED}$, is reported in order to emphasize the effect of the nature of the defect on the change of local stress transfer efficiency near the broken fiber end. This definition of $< \sigma_f >_{RED}$ has no physical significance, and is employed only to amplify the effect of debonding at the fiber end. It may be a useful variable when investigating the slow growth of debonding.

From *Table 1* one can observe that the average axial fiber stress in the fragment will decrease as the size of the defect increases, and that a transverse matrix crack of the same length as an interfacial debond will result in lower stress transfer to the fiber fragment than that occurring with the debond. The fiber efficiency for the fragments possessing both defects is lower than either of the other two cases, as one would expect. The overall changes in fiber efficiency of the fragment are relatively modest compared to the differences in stress profiles at the fiber ends. In the latter case, the differences in the nature of the defects will have a substantial effect on further propagation of the defect, and thus be closely related to the durability of the material.

A case study revisited — the effect of fiber surface treatments on interfacial debonding in epoxy/glass fiber microcomposites

In a previous publication [4] we presented a study of the effects of a number of fiber surface treatments on the fracture toughness of the fiber–matrix interfaces, (called G_{ARREST} in that paper) of a series of epoxy–glass fiber microcomposites. The properties of the constituent materials used are shown in *Table 2*. Embedded single fiber composites (SFC) were slowly pulled until the first fiber break was observed. The strain in the sample gauge length (ϵ_b) and the dimensions of the arrested cracks emanating from the broken fiber ends were measured at constant strain. The FE analysis was carried out using an $X = 50\ \mu$m by $Y = 30\ \mu$m mesh. The reported values of G_{ARREST} were obtained from the strain at break and the crack dimensions using the relation for a linear elastic analysis:

$$G_{\varepsilon_b} = \left(\frac{\varepsilon_b}{0.01}\right)^2 G_{\varepsilon=0.01} \qquad (6)$$

Details of the experimental procedure and FE analysis are reported in the original paper[4]. From a plot of G versus debond length obtained from a finite element analysis of the test, such as shown in *Figure 2*(a) and eqn (6), one can calculate an experimental value of G using measured values of the strain-to-first-break of the fiber and the resulting debond length at constant strain. While we refer to this calculated value as $G_{DYNAMIC}$, the finite element analysis has not included either frictional effects, since a friction coefficient is not obtainable from the experiment, or dynamic effects, since they are not easily evaluated with any degree of precision. The effect of these factors on the probable magnitude of G are discussed below. Those results for

Table 2 Composites constituent material properties used for the FE analysis.

Material	Surface treatment	Tensile modulus (GPa)	Poisson's ratio
S-glass fiber	Starch Soft epoxy coating Methyltrimethoxysilane	86.9	0.22
E-glass fiber	Methyltrimethoxysilane	72.0	0.22
Stiff epoxy	-	2.70	0.35
Soft epoxy	-	1.35	0.35

Table 3 $G_{DYNAMIC}$ values for the fiber–matrix debonding obtained with a $50 \times 30\ \mu m^{24}$ and a $200 \times 100 \mu m^2$ FE model. Strain at first fiber break (ε_b) and debonding length (L_d) are also reported. The FE analysis was linear-elastic

Cases	Epoxy/glass	Fiber surface treatment	ε_b (%)	L_d (μm)	$G_{DYNAMIC}$ (J/m^2) FE model size $X = 50\ \mu$m; $Y = 30\ \mu$m	$G_{DYNAMIC}$ (J/m^2) FE model size $X = 200\ \mu$m; $Y = 100\ \mu$m
A	Stiff/S	Starch	5.2 ± 0.5	5.6 ± 0.3	318 ± 62	447 ± 87
B	Stiff/S	Soft epoxy coating	4.8 ± 0.4	5.5 ± 0.6	273 ± 48	381 ± 67
C	Stiff/S	Methyltrimethoxysilane	4.6 ± 0.3	9.4 ± 1.0	187 ± 27	289 ± 42
D	Soft/S	Starch	6.1 ± 0.7	9.2 ± 1.0	231 ± 56	573 ± 138
E	Soft/S	Soft epoxy coating	5.8 ± 0.6	9.3 ± 0.8.	209 ± 45	517 ± 111
F	Soft/S	Methyltrimethoxysilane	5.1 ± 0.4	14.2 ± 2.3	120 ± 24	336 + 67
G	Stiff/E	Methyltrimethoxysilane	2.5 ± 0.2	3.9 ± 0.6	96 ± 18	142 ± 27
H	Soft/E	Methyltrimethoxysilane	2.4 ± 0.2	5.8 ± 0.4	50 ± 9	128 ± 23

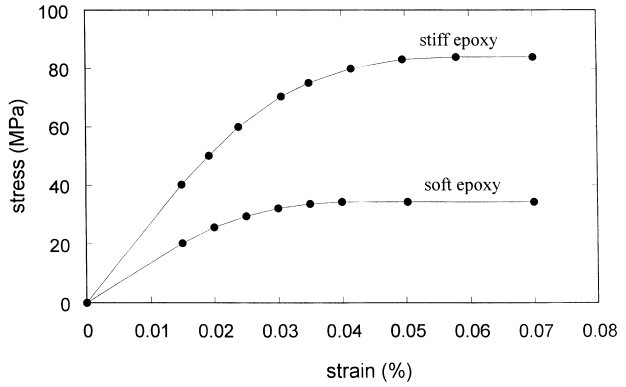

Figure 8 Experimental stress–strain curves for the stiff and soft epoxy matrices considered for the elastoplastic FE analysis

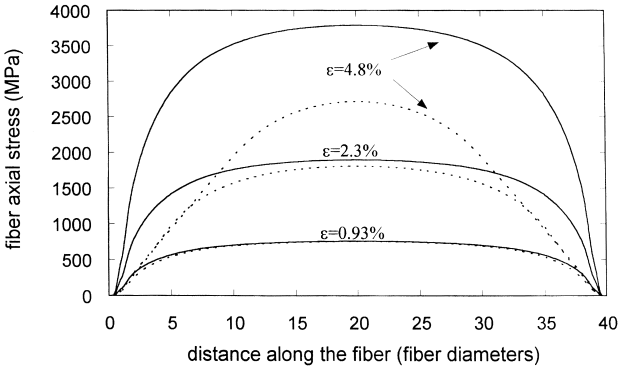

Figure 9 Axial fiber stress profiles as a function of strain for the elastic (———) and elastoplastic (- - -) analyses using an $X = 20$ fiber diameters, $Y = 10$ fiber diameters mesh for an S-glass fiber embedded in the stiff epoxy matrix (case C of *Table 3*)

which interfacial debonding was the only damage mechanism are compared with the analyses presented above. *Table 3* shows a comparison with a linear-elastic FE model using a mesh with $X \geq 200\ \mu$m, $Y \geq 100\ \mu$m, where the results are independent of the mesh size. The values of $G_{DYNAMIC}$ follow the same trends, but are 1.4–2.5 times higher for the larger mesh.

Limitations on the values reported for $G_{DYNAMIC}$

The linear-elastic finite element analysis presented above ignores several of the energy contributions shown in eqn (1). The factors that militate against considering the values of $G_{DYNAMIC}$ reported in *Table 3* as ''absolute'' material properties are neglect of the true elastoplastic or viscoelastic properties of the matrix, the dynamic transient events that occur upon the fracture of the fiber filament and the frictional resistance encountered when a newly broken fiber end retracts into the matrix. The effects of these factors are briefly considered below.

Effect of elastoplastic behavior on calculation of $G_{DYNAMIC}$. The most serious question concerning the calculation of the interface properties is whether or not a linear elastic analysis is appropriate when one is dealing with an elastoplastic or viscoelastic matrix. *Figure 8* shows stress–strain curves for the two epoxy matrices used in these studies. Beyond a strain of 1–2%, the matrices are clearly non-linear. Thus, the stored energy available for driving defects upon the fracture of a filament (at 2.5% average for E-glass or 5.2% average for S-glass) is considerably less than that obtained using a linearelastic analysis. The FE analysis was repeated for the specific cases presented

Table 4 Values of $G_{DYNAMIC}$, and the ratio $G_{DYNAMIC}/ < \sigma_f >_b$ for the fiber–matrix debonding obtained with a 200 × 100 μm^2 FE model. An elastoplastic naatrix behaviour was considered in the FE analysis

Cases	Epoxy/Glass	Fiber surface treatment	$G_{DYNAMIC}$ (J/m^2)	$G_{DYNAMIC}/ < \sigma_f >_b$ (J/m^{2}GPa^{-1})
A	Stiff/S	Starch	258	57
B	Stiff/S	Soft epoxy coating	230	55
C	Stiff/S	Methyltrimethoxysilane	219	55
G	Stiff/E	Methyltrimethoxysilane	86	48
D	Soft/S	Starch	193	36
E	Soft/S	Soft epoxy coating	185	37
F	Soft/S	Methyltrimethoxysilane	138	31
H	Soft/E	Methyltrimethoxysilane	60	35

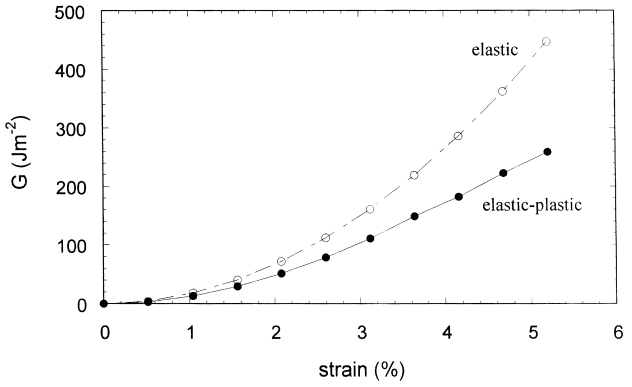

Figure 10 Values of G as a function of strain for the case A of *Tables 3 and 4*. Both linear elastic and elastoplastic analyses are reported

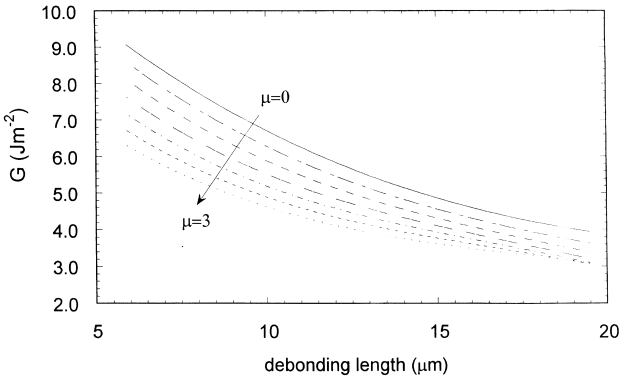

Figure 11 Effect of the fiber–matrix coefficient of friction on the strain energy release rate vs debond length curves for a S-glass fiber embedded in an elastic matrix with a modulus of 1.6 GPa, at 1% of strain. The FE model size is $X = 50$ μm, $Y = 30$ μm (after DiBenedetto and Gurvich[10])

above (see *Table 3*), using the elastoplastic modelling facility of MARC by considering the actual material properties and the von Mises yield criterion. *Figure 9* compares the axial fiber stress profiles as a function of strain for the elastic and elastoplastic analyses, using an $X = 20$ fiber diameters, $Y = 10$ fiber diameters mesh. There is a clear diminution of the stress transfer at strain levels higher than about 1%. The decrease is even more pronounced when examining the calculated values of $G_{DYNAMIC}$, which will be proportional to ε_b^2 in the elastic case and to ε_b. in the limit of ideal plastic response (i.e. yielding at constant stress). *Figure 10* is a comparison of G as a function of strain for the case A of *Table 3*. It is evident that after about 3% strain G is an almost linear function of the strain. The values of $G_{DYNAMIC}$, and the ratio $G_{DYNAMIC}/ < \sigma_f >_b$ for the eight cases shown in *Table 3* are reported in *Table 4*. The values for $G_{DYNAMIC}$ are substantially lower than those calculated using an equivalent linear-elastic statement. Most important, the ratio, $G_{DYNAMIC}/ < \sigma_f >_b$ is nearly constant for all cases employing the same matrix, indicating that the calculated values of $G_{DYNAMIC}$ are a function of the strain level at which the first fiber fracture occurred, and suggesting that the stiffness and strength of the matrix phase are the primary factors controlling the interface dynamic toughness.

The transient dynamic events following filament fracture. In a previous study, the dynamic effects associated with fiber breakage in single- and multiple-fiber microcomposites were investigated using finite element simulation[11]. The dynamic stresses were shown to be significantly different from the calculated static stresses and, consequently, have an effect on the subsequent damage occuring following filament fracture. For single fiber microcomposites, the dynamic stresses generated by a single filament fracture overshoot the static equilibrium values within nanoseconds and then oscillate around equilibrium. The amplification of all components of the stress vector along the fiber–matrix interface is approximately equal and thus the dynamic stress state can be characterized by a single dynamic amplification factor (DAF). For the single-glass fiber–epoxy microcomposites investigated, the DAF values were in the range of 1.02–1.15 and reached the maximum within 15–50 ns. Thus, it is reasonable to assume that calculations of strain energy release rates from equilibrium stress profiles, using measurements of debond or matrix crack lengths, following a filament fracture, will be different than those calculated for the slow propagation of an existing defect. The dynamic process is accompanied by a higher initiation force and kinetic energy changes not usually accounted for in these analyses. Both factors will tend to drive the crack farther than would be expected when an existing natural crack advances slowly under constant load. Thus, in general, one would expect the calculated value of $G_{DYNAMIC}$ to be different than a critical value of strain energy release rate, $(G_C)_{PROPAGATION} = R$, as defined in a traditional fracture mechanics test. This situation is similar to that observed when studying materials under impact loading[12].

Frictional effects. When a filament in a composite breaks, a Poisson contraction of the matrix at the broken end produces an additional radial compression on the fiber that

promotes a strong frictional resistance to retraction of the fiber in the matrix. The radial stress increases in proportion to the axial stress in the fiber and, thus, creates a work of friction that increases as the strain-to-break of the filament increases. When frictional forces are included in the FE analysis, less of the released elastic energy is available for driving the defects, thereby decreasing the calculated value of G_{DYNAMIC}. *Figure 11* shows the effect of friction on the calculated values of G_{DYNAMIC} for debonding of an elastic matrix, $E_{\mathrm{m}} = 1.6$ GPa, from an S-glass fiber at 1% strain as a function of the frictional coefficient at the interface[10]. Since the embedded fiber fragmentation geometry is not suited to measuring a friction coefficient, this effect was not included in the above analyses. If the friction coefficients are in a ''normal'' range of $\mu < 2$, the overall effect is relatively small.

CONCLUSIONS

In this work the finite element (FE) method has been used to evaluate the axial fiber stress profiles and energy changes accompanying interfacial debonding and/or matrix cracking following a single fiber fragmentation event. The observed fracture events were simulated using both elastic and elastoplastic FE axisymmetrical models. Axial fiber stress profiles for debonding, matrix cracking and combined debonding/matrix cracking were determined. While the average axial fiber stress is only modestly affected by the nature of the defect, the stress profiles near the fragment ends are substantially different and can best be characterized using the concept of ''imperfect interfaces''.

The effects of the model size and material properties on the strain energy release rate, G, associated with interfacial debonding and matrix cracking have also been assessed. Due to the specific boundary conditions chosen, a size independent value of G can be attained provided that the radial dimension extends to at least 10 fiber diameters and the half-fragment length is greater than approximately 20 fiber diameters. A case study has been revisited in the light of above statements, and strain energy release rates for the dynamic initiation, growth and arrest of an interfacial debond, G_{DYNAMIC}, were calculated for various fiber–matrix combinations. Above about 1% strain, elastoplastic FE analysis of the debonding occurring immediately after the fracture of single glass fibers embedded in epoxy matrices resulted in lower values of average axial fiber stress and G_{DYNAMIC} when compared to those obtained using a linear-elastic analysis. The calculated strain energy release rates, G, were proportional to $\varepsilon_{\mathrm{b}}^2$ below $\varepsilon_{\mathrm{b}} = 0.01$ and to ε_{b} above $\varepsilon_{\mathrm{b}} = 0.03$. The calculated G_{DYNAMIC} values were found to be proportional to the stress at which the first fiber fracture occurred and therefore were not independent of the state of stress within the test specimen.

REFERENCES

1. Hashin, Z., Thermoelastic properties of fiber composites with imperfect interface. *Mech. Mater.*, 1990, **8**, 333.
2. Nairn, J.A. and Liu, Y.C., Stress transfer into a fragmented, anisotropic fiber through an imperfect interface. *Int. J. Solids Structures*, 1997, **34**, 1255.
3. Wagner, H.D., Nairn, J.A. and Detassis, M., Toughness of interfaces from initial fiber–matrix debonding in a single fiber composite fragmentation test. *Appl. Comput. Math.*, 1995, **2**, 107.
4. Pegoretti, A., Accorsi, M.L and DiBenedetto, A.T., Fracture toughness of the fibre–matrix interface in glass–epoxy composites. *J. Mater. Sci.*, 1996, **31**, 6145.
5. Copponex, T.J., Analysis and evaluation of the single.fibre fragmentation test. *Comput. Sci. Technol.*, 1996, **56**, 893.
6. Tripathi, D. and Jones, F.R., Measurement of the load-bearing capability of the fibre–matrix interface by single-fibre fragmentation. *Comput. Sci. Technol.*, 1997, **575**, 925.
7. Tripathi, D., Chen, F. and Jones, F.R., The effect of matrix plasticity on the stress fields in a single filament composite and the value of interfacial shear strength obtained from the fragmentation test. *Proc. R. Soc. Lond. A*, 1996, **452**, 621.
8. Nath, R.B., Fenner, D.N. and Galiotis, C., Elastoplastic finite element modelling of interfacial failure in model Kevlar 49 fibre–epoxy composites. *Composites Part A*, 1996, **27A**, 821.
9. Pegoretti, A., Fidanza, M., Migliaresi, C. and DiBenedetto, A.T., Toughness of the fiber matrix interface in nylon-6/glass fiber composites. *Composites Part A*, 1998, **29A**, 283.
10. DiBenedetto, A.T. and Gurvich, M.R., Effect of friction between fiber and matrix on fracture toughness of the composite interface. *J. Mater. Sci.*, 1998, **33**, 000.
11. Accorsi, M.L., Pegoretti, A. and DiBenedetto, A.T., Dynamic analysis of fibre breakage in single- and multiple-fibre composites. *J. Mater. Sci*, 1996, **31**, 4181.
12. Broek, D., *Elementary Engineering Fracture Mechanics*, Martinus Nijhoff, Dordrecht, 1986, p. 150.
13. DiAnselmo, A., Accorsi, M.L. and DiBenedetto, A.T., The effect of an interphase on the stress and energy distribution in the embedded single fibre test. *Comput. Sci. Technol.*, 1992, **44**, 215.
14. DiBenedetto, A.T., Connelly, S.M., Lee, W.C. and Accorsi, M.L., The properties of organosiloxane/polyester interfaces at an E-glass fiber surface. *J. Adhesion*, 1995, **52**, 41.
15. Detassis, M., Frydman, E., Vrieling, D., Zhou, X.R., Wagner, H.D. and Nairn, J.A., Interface toughness in fibre composites by the fragmentation test. *Composites Part A*, 1996, **27A**, 769.
16. Kelly, A. and Tyson, W.R., Tensile properties of fiber-reinforced metals/copper/tungsten and copper/molybdenum. *J Mech. Phys. Solids*, 1965, **135**, 329.
17. Cox, H.L., The elasticity and strength of paper and other fibrous materials. *Br. J. Appl. Phys.*, 1952, **3**, 72.